OPEN

Paravascular microcirculation facilitates rapid lipid transport and astrocyte signaling in the brain

Vinita Rangroo Thrane[1,2,3]*, Alexander S. Thrane[1,2,3]*, Benjamin A. Plog[1],
Meenakshisundaram Thiyagarajan[1], Jeffrey J. Iliff[1], Rashid Deane[1], Erlend A. Nagelhus[2,3]
& Maiken Nedergaard[1]

[1]Division of Glia Disease and Therapeutics, Center for Translational Neuromedicine, Department of Neurosurgery, University of Rochester Medical Center, Rochester, New York 14642, [2]Letten Institute of Basic Medical Sciences, University of Oslo, 0317 Oslo, Norway, [3]Centre for Molecular Medicine Norway, Nordic EMBL Partnership, University of Oslo, 0318 Oslo, Norway.

In the brain, a paravascular space exists between vascular cells and astroglial end-foot processes, creating a continuous sheath surrounding blood vessels. Using *in vivo* two-photon imaging we demonstrate that the paravascular circulation facilitates selective transport of small lipophilic molecules, rapid interstitial fluid movement and widespread glial calcium signaling. Depressurizing the paravascular system leads to unselective lipid diffusion, intracellular lipid accumulation and pathological signaling in astrocytes. As the central nervous system is devoid of lymphatic vessels, the paravascular space may serve as a lymphatic equivalent that represents a separate highway for the transport of lipids and signaling molecules.

The brain, unlike other organs, lacks a separate lymphatic system to clear interstitial fluid, transport lipids and facilitate diffusion of signaling molecules. In addition to the neuropil being isolated from the systemic circulation by the blood-brain barrier, the narrow and highly tortuous extracellular space is incompatible with rapid fluid and solute movement[1–3]. Despite these impediments, the brain has a high interstitial fluid turnover rate that has recently been shown to depend on cerebrospinal fluid (CSF) circulation via the paravascular space[4,5]. This anatomical space is completely ensheathed by astrocyte endfeet and is well positioned to serve as a highway for glial-glial and glial-vascular communication[1,6,7]. However, the role of the paravascular space in lipid transport and signal transduction has not been investigated *in vivo*. Two related questions therefore remain unanswered: can the paravascular space facilitate rapid lipid transport and might this space act as a separate compartment for astrocyte signaling?

Results

To outline the CSF microcirculation, tracers were infused via the cisterna magna (**Fig. 1a**). Both the fixable lipophilic tracer Texas red hydrazide (TXR, 0.621 kDa) and the hydrophilic tracer tetramethylrhodamine (TMR, 3 kDa) moved rapidly through the brain along cerebral blood vessels (tracer penetration: TXR 12.57 ± 4.41 and TMR $38.71 \pm 7.70\%$ brain area at 30 min). Surprisingly, lipophilic tracers of small molecular weight showed as limited parenchymal penetration as large hydrophilic tracers (fluorescein isothiocyanate dextran, FITC, 2000 kDa) in cortical grey matter (tracer penetration $15.56 \pm 2.81\%$ brain area) (**Fig. 1b, c**)[4,5].

We used *in vivo* two-photon laser scanning microscopy (2PLSM) to further explore the highly selective paravascular movement of lipophilic tracers. This restricted movement is unexpected as biologically relevant lipid molecules, such as prostaglandins, cholesterol and palmitic acid, are small (< 1 kDa) and cell permeable[8–12]. We demonstrated that the movement of small (< 1 kDa) lipophilic tracers was highly selective to the paravascular space (palmitic acid, rhod-2, TXR, sulforhodamine SR101 and Oregon green BAPTA-1 OGB) (**Fig. 2a, Supplementary Fig. 1a**). Intra-arterial Texas red dextran or FITC were used to morphologically distinguish cortical surface arteries and veins as well as penetrating arterioles and venules (**Supplementary Fig. 1a**)[4]. Cross-sectional intensity projections of penetrating arterioles confirmed paravascular tracer selectivity (**Fig. 2b**). By analyzing regions of interest representing the paravascular space and the surrounding tissue (**Fig. 2c**), we showed that the lipophilic tracers were rapidly cleared via the paravascular space without gaining access to the surrounding tissue (normalized tracer fluorescence ratio of paravascular space to surround at 60 min: OGB 3.36 ± 0.79,
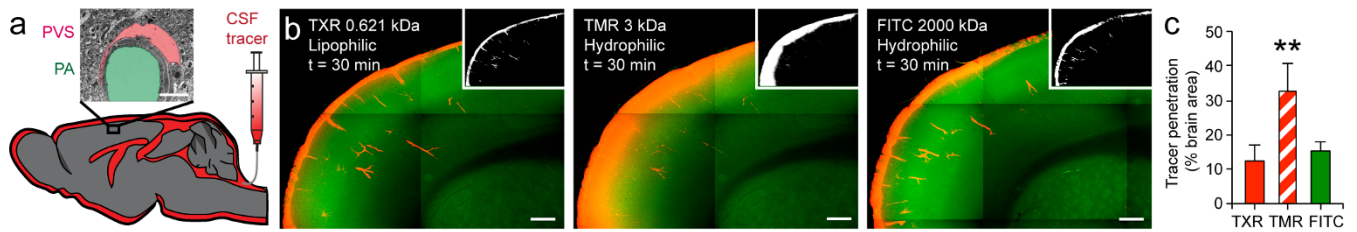
Figure 1 | Rapid paravascular movement of lipophilic tracers. (a) Experimental design for studying tracer (red) movement in paravascular space via cisterna magna. Inset: electron micrograph of penetrating arteriole (PA) with surrounding paravascular space (PVS). Scale bar represents 2.5 μm. (b) Epifluorescence montages illustrate distribution of Texas red hydrazide (TXR), fluorescein isothiocyanate dextran (FITC) and tetramethylrhodamine dextran (TMR). Top insets display auto-thresholded images. Scale bar represents 200 μm. (c) Quantification of brain parenchymal penetration. **$P < 0.01$, $n = 6$ animals for all groups, Mann-Whitney U. Data are shown as mean $\pm$ SEM.

SR101 3.50 ± 0.88, rhod-2 4.21 ± 1.35) **(Fig. 2d)**. Deletion of the astrocyte water channel aquaporin-4 has recently been shown to slow the circulation of hydrophilic tracers in CSF, but did not affect lipophilic tracer movement (paravascular space to surround ratio in $Aqp4^{-/-}$ at 60 min: 4.83 ± 1.42)[4].

We next examined whether lipophilic tracers enter and exit the brain via similar arterio-venous paravascular routes as hydrophilic molecules[4]. Using NG2-DsRed mice that have fluorescently labeled vascular smooth muscle in arterioles, we showed that the biologically relevant tracer palmitic acid entered via a para-arterial route
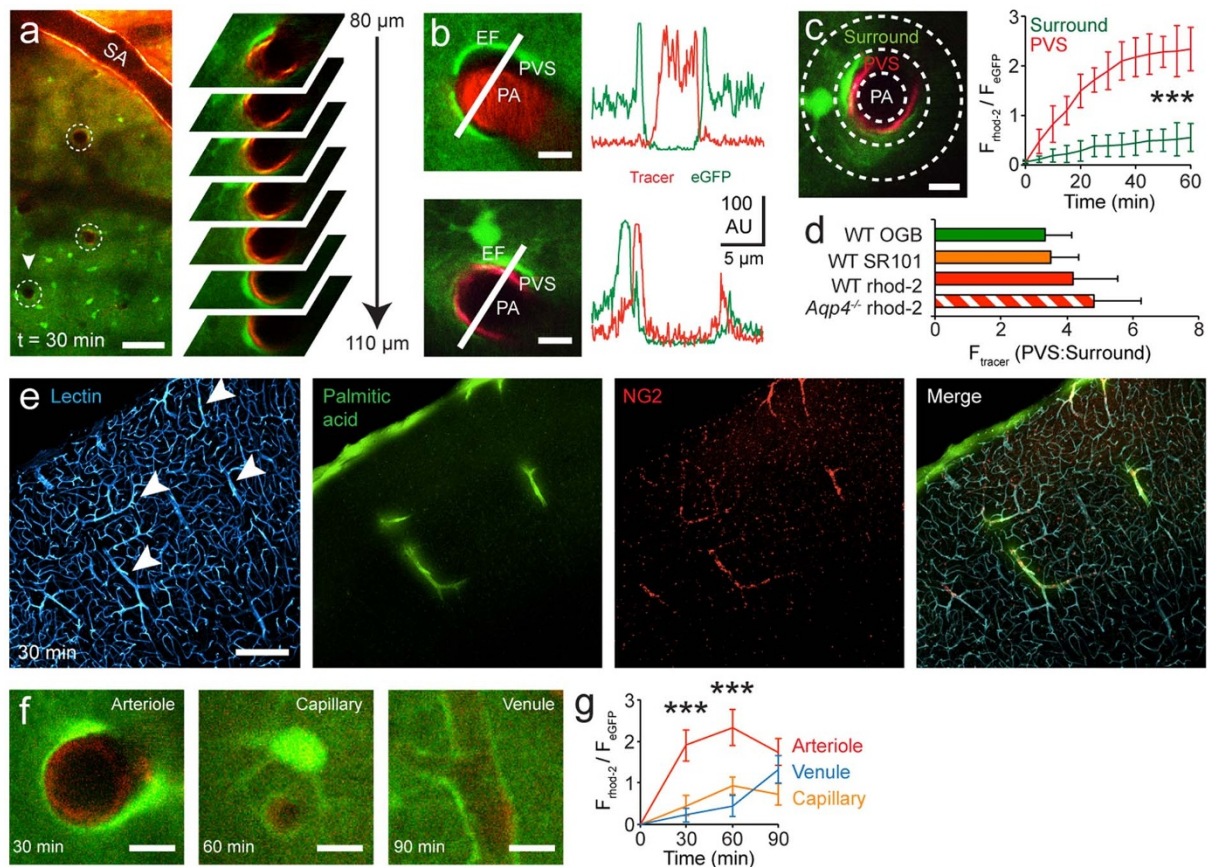
Figure 2 | Lipophilic tracers selectively enter and exit brain via paravascular space surrounding arterioles and venules. (a) Left: *in vivo* two-photon image of rhod-2 circulation via the paravascular space in *Glt1*-eGFP mouse. White circles indicate penetrating arterioles. Surface artery (SA). Scale bar represents 100 μm. Right: high magnification images of the paravascular space surrounding penetrating arteriole at serial depths. (b) Cross sectional intensity traces illustrating the paravascular space (rhod-2, red) and intravascular space (Texas red dextran) around a penetrating arteriole (PA). Endfoot (EF). Scale bar represents 7.5 (top) and 5 (bottom) μm. (c) Region of interest (left) and analysis of tracer intensity (right) in the paravascular space and surrounding parenchyma. Scale bar represents 10 μm. $n = 24$ arterioles from 7 animals, paired t test. (d) Ratio of lipophilic tracer fluorescence in paravascular space to surrounding parenchyma at 60 min. Sulforhodamine (SR101), Oregon green BAPTA (OGB). $n = 11$ (OGB), 15 (SR101), 24 (rhod-2) and 12 ($Aqp4^{-/-}$ rhod-2) arterioles from 16 animals (total), unpaired t test. (e) Immunofluorescence micrographs from NG2-DsRed mouse show entry of palmitic acid lipid along the paravascular space. Antibody against lectin outlines vascular endothelium. White arrows indicate arterioles. Scale bar represents 100 μm. (f, g) Representative images and quantification of rhod-2 tracer in the paravascular space surrounding an arteriole, a capillary and venule. Scale bars represent 7.5 μm. $n = 24$ (arterioles), 14 (capillaries) and 12 (venules) from 7 animals, paired t test. ***$P < 0.001$. Data are shown as mean $\pm$ SEM.

(Fig. 2e). Moreover, using 2PLSM imaging we showed that lipophilic tracer (rhod-2) moved sequentially in the paravascular space surrounding surface arteries, penetrating arterioles, capillaries and venules following cisterna magna infusion (normalized fluorescence of rhod-2 to eGFP expressed under the astrocyte specific *Glt1* promoter: 30 min: arteriole 1.90 ± 0.38, capillary 0.45 ± 0.247, venule 0.23 ± 0.172; 60 min: arteriole 2.34 ± 0.44, capillary 0.94 ± 0.21, venule 0.44 ± 0.25; 90 min: arteriole 1.74 ± 0.32, capillary 0.72 ± 0.27, venule 1.33 ± 0.34) (Fig. 2f, g). These observations indicate that lipophilic molecules enter the brain via para-arterial and exit via para-venous routes.

To investigate the consequences of disrupting the paravascular microcirculation, we temporarily depressurized the CSF compartment by puncturing the cisterna magna (CMP) (Fig. 3a). Previous studies have shown that this procedure depletes ventricular and subarachnoid CSF circulation[13]. Using 2PLSM to image paravascular tracer movement we demonstrate that CMP also drains all tracer from the PVS (normalized fluorescence of rhod-2 to eGFP before 4.21 ± 1.35 vs. after CMP 0.24 ± 0.15) (Fig. 3b).

Since the paravascular CSF circulation appears to prevent unspecific lipid diffusion into the brain parenchyma, we next hypothesized that CMP might accelerate lipid tracer accumulation in the parenchyma. We took advantage of astrocyte specific calcium indicators (such as rhod-2), which are lipophilic tracers that become concentrated inside cells due to their acetoxymethyl group[14,15]. This improved the sensitivity for detecting parenchymal influx. We found that CMP accelerates intracellular accumulation of lipophilic tracer rhod-2, when this was applied to the cortical surface or injected intraparenchymally (eGFP normalized fluorescence of rhod-2 astrocyte labeling intensity at 30 min for sham control: 1.54 ± 0.36 vs. CMP: 4.01 ± 0.57) (Fig. 3c, d). Conversely, *Aqp4* deletion, which slows paravascular water movement, did not enhance cellular tracer uptake ($Aqp4^{-/-}$ control at 30 min: 1.56 ± 0.27) (Fig. 3e). Thus, an intact paravascular space restricts lipid diffusion and cellular uptake.
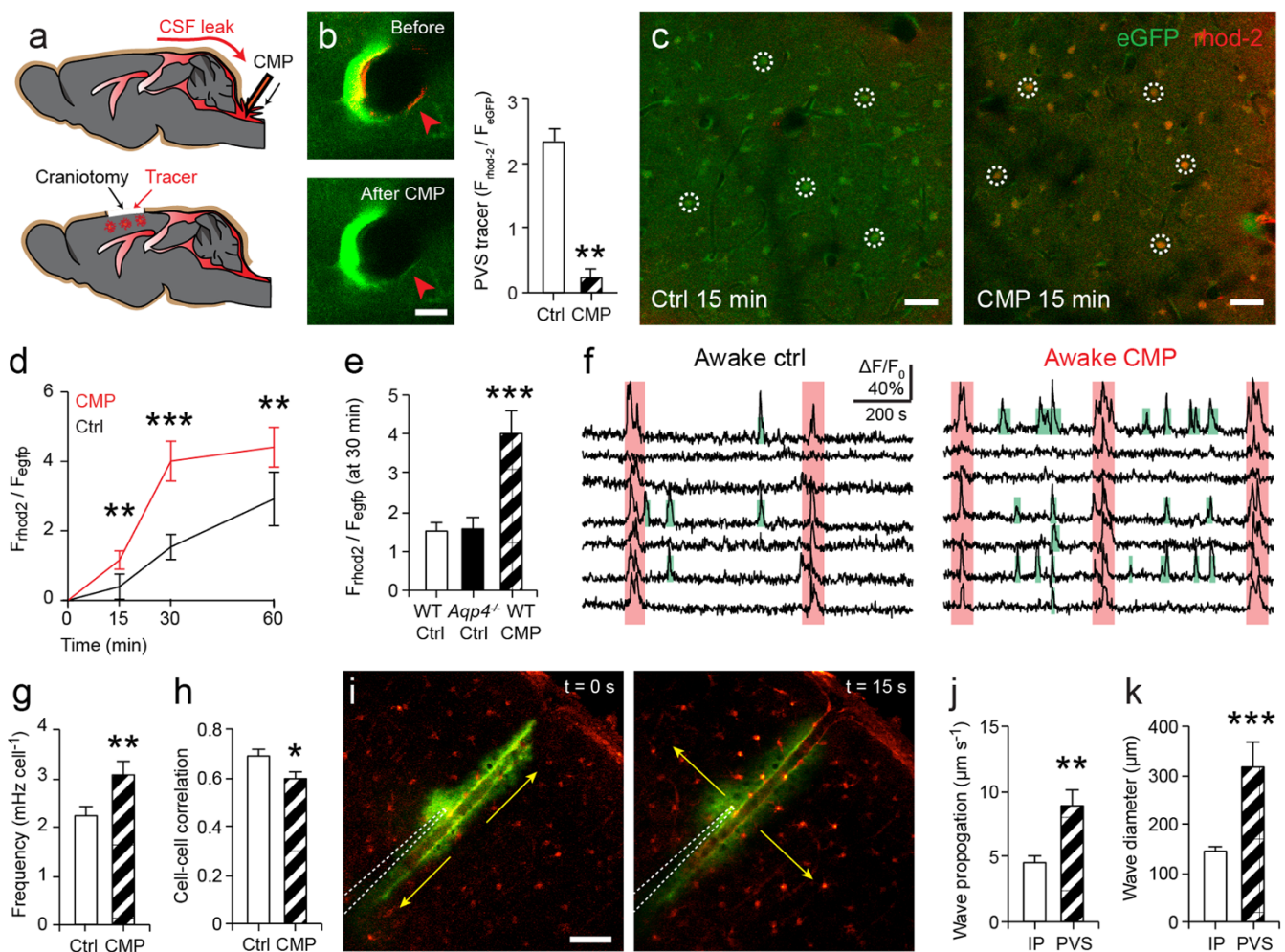
Figure 3 | Depressurizing the paravascular space impairs lipid transport and astrocyte signaling. (a) Cisterna magna puncture (CMP) temporarily depressurizes the paravascular space. Lipophilic tracer (rhod-2) was applied to cortical surface or injected into parenchyma to assess tissue influx. (b) Cisterna magna puncture (CMP) drains nearly all paravascular tracer (rhod-2). $n = 7$ arterioles from 2 animals, Wilcoxon signed ranks test. Scale bar represents 10 μm. (c, d) Two-photon images and quantification of lipid tracer labeling in eGFP expressing cortical astrocytes (circled) following sham control and cisterna magna puncture (CMP). Scale bars represent 75 μm. $n = 45$ cells from 5 animals for both groups, unpaired t test. (e) Normalized rhod-2 astrocyte labeling intensity. $n = 45$ (Ctrl), 32 ($Aqp4^{-/-}$) and 45 (CMP) cells from 14 animals (total), one-way ANOVA. (f) Representative traces of spontaneous calcium activity from cortical astrocytes in awake mice. Synchronized (red) and individual (green) transients. (g, h) CMP increases frequency and reduces synchronization of astrocyte calcium signals. $n = 60$ (ctrl) and 52 (CMP) cells from 10 animals (total), unpaired t test. (i–k) ATP injection (visualized with FITC-dextran) into the paravascular space stimulates rapid and widespread astrocyte calcium wave spreading outwards from the blood vessel. $n = 16$ (intraparenchymal, IP) and 9 (paravascular space, PVS) slices from 11 animals (total), unpaired t test. Scale bar represents 40 μm. *$P < 0.05$, **$P < 0.01$, ***$P < 0.001$. Data are shown as mean ± SEM.

To investigate the role of the paravascular space as a signaling compartment, we compared spontaneous astrocyte calcium activity in the cortex of awake mice subjected to CMP or sham surgery. Interestingly, depressurizing the paravascular space caused increased frequency and decreased synchronization of calcium signaling (ctrl 2.21 ± 0.19 vs. CMP 3.08 ± 0.29 mHz cell^{-1}; cell-cell correlation: ctrl 0.69 ± 0.03 vs. CMP 0.60 ± 0.03) (Fig. 3f–h)[15]. Other aspects of astrocyte signaling were not affected (amplitude: ctrl 39.08 ± 2.10% vs. CMP 39.98 ± 2.18%; duration: ctrl 21.29 ± 1.29 s vs. CMP 24.74 ± 1.62 s; P(active over 15 min): ctrl 75.83 ± 4.20% vs. CMP 7981.05 ± 4.18%) (Supplementary Fig. 1b–d). Astrocyte calcium activity has been shown to propagate along blood vessels and the waves are largely ATP mediated[16–19]. We therefore inserted a microelectrode into the paravascular space *in situ* and stimulated calcium transients by injecting ATP. The rapid movement of agonist in the paravascular space stimulated a brisk calcium wave spreading outwards from the blood vessel, which propagated faster and over a larger area than when ATP was injected intraparenchymally (wave propagation: parenchyma 4.47 ± 0.56 vs. paravascular space 8.89 ± 1.22 μm s^{-1}; wave diameter: parenchyma 142.86 ± 12.50 vs. paravascular space 315.81 ± 51.42 μm) (Fig. 3i–k).

Discussion

To summarize, we show that the brain has a distinct paravascular compartment for lipid transport and glial signaling within the narrow confines of the neuropil. Lipid transport follows the arteriovenous circulation and is highly selective to the paravascular space. Compromising paravascular transport causes increased intracellular lipid accumulation and abnormal astrocyte calcium signaling. We speculate that lipid transport in the brain may be spatially restricted due to the high concentration of astrocyte-secreted lipoproteins in CSF. Interestingly, lipoprotein mutations are the largest known risk factor for developing Alzheimer disease[20,21]. Ours and previous data therefore suggest that the paravascular compartment may represent a lymphatic equivalent in the brain that resorbs interstitial fluid, selectively transports small lipid molecules and can act as a signaling highway for coordinated astrocyte communication.

Methods

Animals. Glt-1-eGFP, NG2-DsRed and *Aqp4*$^{-/-}$ mice were generated as outlined previously[4,17], and mice of either sex from 6–12 weeks used in conjunction with C57BL/6J wild-types (Jackson Laboratories) were used for experiments. All animals, except those used for awake imaging, were anesthetized with ketamine (0.12 mg g^{-1}) and xylazine (0.01 mg g^{-1}) intraperitoneally (i.p.). All animal experiments were approved by the Animal Care and Use Committee of the University of Rochester.

Tracer preparation and intracisternal infusion. The hydrophilic tracers fluorescein isothiocyanate (FITC) dextran (0.5%, 2000 kDa) and tetramethylrhodamine (TMR) dextran (0.5%, 3 kDa) and the lipophilic, cell-permeant tracers palmitic acid (BODIPY® FL C$_{16}$ 1 mg ml^{-1}, 0.474 kDa, Molecular Probes), Texas red hydrazide (0.4–2 mM, 0.621 kDa), sulforhodamine SR101 acid chloride (0.2 mM, 0.607 kDa), rhod-2 acetoxymethyl (AM) (0.45–4.5 mM, 1.124 kDa) and Oregon-green BAPTA-1 (OGB) AM (0.5 mM, 1.258 kDa, acquired from Invitrogen and Sigma-Aldrich) were constituted in artificial cerebrospinal fluid (aCSF)[17]. These tracers were chosen because of their small size (comparable to endogenous lipids), relevance to *in vivo* imaging (e.g. as calcium indicators) and ability to cross cell membranes, such as the endfoot membrane that encases the paravascular space[15,17]. The mice were secured in a stereotaxic frame, and a 30G needle was inserted into the cisterna magna. Tracer dissolved in aCSF was delivered at a rate of 2 μL min^{-1} over 5 minutes with a syringe pump (Harvard Apparatus). The dyes were used at higher concentrations than direct cortical application to allow the approximate dilution factor of 1:5 when 10 μL was infused into the total mouse CSF volume of 40 μL[22]. The cisterna magna was punctured with a 30G needle to drain the CSF and depressurize the paravascular space. In sham control animals the cisterna magna was exposed without puncturing it.

***Ex vivo* imaging.** Mouse preparation was modified from published protocols[4]. The animals were perfused transcardially with 4% paraformaldehyde in 0.1 M phosphate buffered saline (pH 7.4) and post-fixed overnight. 100 μm vibratome brain sections were then cut and mounted on slides using PROLONG anti-fade gold with DAPI (Invitrogen). Epifluorescence multi-channel whole-brain montages were collected using a virtual slice module (Microlucida Software, Microbrightfield). Exposure and

gain levels were maintained constant throughout the study. The percentage of brain tracer penetration was calculated using the area fraction function in ImageJ (NIH) on consistently thresholded images, as described previously[4]. For EM experiments 0.1% glutaraldehyde was added to the perfusate/fixation solution and the ultra-thin Lowicryl sections were prepared as outlined previously[23]. Images were obtained 125 μm below the surface in the barrel cortex.

***In vivo* imaging.** Anesthetized animals were intubated and artificially ventilated with a small animal ventilator (CWE), their temperature was maintained using a heating pad, and blood gasses were collected via a femoral arterial cannula to ensure physiological hemodynamic parameters[17]. To visualize the cerebral vasculature FITC or Texas red dextran (Invitrogen) were administered intra-arterially. A steel frame was secured to the skull using dental cement, and a 2 mm craniotomy was opened over the somatosensory cortex with particular care being taken not to puncture the dura mater. To stabilize imaging, the craniotomy was then sealed with agarose (1.5%, type III-A, Sigma) and a coverslip. A Mai Tai laser (SpectraPhysics) attached to a confocal scanning system (Fluoview 300, Olympus) and an upright microscope (IX51 W) were used. Tracers and eGFP were excited at 850–890 nm and emission was collected at 575–645 nm using a 20x (0.95NA) lens. 512 × 512 pixel frames were collected from the pial surface to 200 μm depth at 20 μm z-steps. Superficial arteries and veins were distinguished based on morphology (e.g. arteries pass more superficially, and have fewer branches near the surface)[4]. Tracer movement was analyzed as outlined previously by defining doughnut shaped ROIs around cerebral blood vessels[4].

Awake calcium imaging. Animal preparation was performed as described by the authors previously[15]. Briefly, mice were anesthetized with isoflurane (1.0–1.5%), head-restrained with a steel mini-frame, and habituated to imaging through training sessions. The craniotomy was made as outlined above and rhod-2 (2 mM, Invitrogen) was loaded onto exposed cortex before applying the coverslip. Calcium signaling was imaged 75–125 μm depth and dual channel (rhod-2 and eGFP) frames were collected at 0.2 or 1 Hz. Calcium transients were analysed using previously described custom-made software (MatLab Inc.) and Image J (NIH)[15,17].

***In situ* calcium imaging.** Acute cortical slices were prepared from P10-20 mice as described previously[16,17]. Briefly, 400 μm acute cortical slices were incubated with rhod-2 (2 mM) for 20 min, before being transferred to a recording chamber where they were imaged and analyzed as outlined before[17]. ATP (500 μM in aCSF) was injected via a glass microelectrode 40–80 μm into the paravascular space or parenchyma of the slice using a picospritzer (10 psi, 100 ms, Parker Instrumentation). We used FITC dextran (1%, 2000 kDa) to visualize the injection.

Statistical analyses. All analysis was performed using IBM SPSS Statistics 19 and all tests were two-tailed where significance was achieved at α = 0.05 level. Wherever necessary a Bonferroni correction for multiple testing was done.

1. Abbott, N. J. Evidence for bulk flow of brain interstitial fluid: significance for physiology and pathology. *Neurochemistry international* **45**, 545–552 (2004).
2. Abbott, N. J., Patabendige, A. A., Dolman, D. E., Yusof, S. R. & Begley, D. J. Structure and function of the blood-brain barrier. *Neurobiology of disease* **37**, 13–25 (2010).
3. Sykova, E. & Nicholson, C. Diffusion in brain extracellular space. *Physiological reviews* **88**, 1277–1340 (2008).
4. Iliff, J. J. *et al.* A Paravascular Pathway Facilitates CSF Flow Through the Brain Parenchyma and the Clearance of Interstitial Solutes, Including Amyloid beta. *Science translational medicine* **4**, 147ra111 (2012).
5. Iliff, J. J. *et al.* Brain-wide pathway for waste clearance captured by contrast-enhanced MRI. *The Journal of clinical investigation* **123**, 1299–1309 (2013).
6. Attwell, D. *et al.* Glial and neuronal control of brain blood flow. *Nature* **468**, 232–243 (2010).
7. Begley, D. J. Brain superhighways. *Science translational medicine* **4**, 147fs129 (2012).
8. Slezak, M. & Pfrieger, F. W. New roles for astrocytes: regulation of CNS synaptogenesis. *Trends in neurosciences* **26**, 531–535 (2003).
9. Moore, C. I. & Cao, R. The hemo-neural hypothesis: on the role of blood flow in information processing. *Journal of neurophysiology* **99**, 2035–2047 (2008).
10. Fukata, Y. & Fukata, M. Protein palmitoylation in neuronal development and synaptic plasticity. *Nature reviews. Neuroscience* **11**, 161–175 (2010).
11. Takano, T. *et al.* Astrocyte-mediated control of cerebral blood flow. *Nat Neurosci* **9**, 260–267 (2006).
12. Higashimori, H., Blanco, V. M., Tuniki, V. R., Falck, J. R. & Filosa, J. A. Role of epoxyeicosatrienoic acids as autocrine metabolites in glutamate-mediated K+ signaling in perivascular astrocytes. *American journal of physiology. Cell physiology* **299**, C1068–1078 (2010).
13. Reiber, H. & Schunck, O. Suboccipital puncture of guinea pigs. *Laboratory animals* **17**, 25–27 (1983).
14. Paredes, R. M., Etzler, J. C., Watts, L. T., Zheng, W. & Lechleiter, J. D. Chemical calcium indicators. *Methods (San Diego, Calif.)* **46**, 143–151 (2008).
15. Thrane, A. S. *et al.* General anesthesia selectively disrupts astrocyte calcium signaling in the awake mouse cortex. *Proceedings of the National Academy of Sciences of the United States of America* **109**, 18974–18979 (2012).

16. Simard, M., Arcuino, G., Takano, T., Liu, Q. S. & Nedergaard, M. Signaling at the gliovascular interface. *J. Neurosci.* **23**, 9254–9264 (2003).

17. Thrane, A. S. *et al.* Critical role of aquaporin-4 (AQP4) in astrocytic Ca2+ signaling events elicited by cerebral edema. *Proc. Natl. Acad. Sci. U. S. A.* **108**, 846–851 (2010).

18. Koizumi, S., Fujishita, K. & Inoue, K. Regulation of cell-to-cell communication mediated by astrocytic ATP in the CNS. *Purinergic signalling* **1**, 211–217 (2005).

19. Parpura, V. & Verkhratsky, A. Homeostatic function of astrocytes: Ca(2+) and Na(+) signalling. *Translational neuroscience* **3**, 334–344 (2012).

20. Leoni, V., Solomon, A. & Kivipelto, M. Links between ApoE, brain cholesterol metabolism, tau and amyloid beta-peptide in patients with cognitive impairment. *Biochemical Society transactions* **38**, 1021–1025 (2010).

21. Castellano, J. M. *et al.* Low-density lipoprotein receptor overexpression enhances the rate of brain-to-blood Abeta clearance in a mouse model of beta-amyloidosis. *Proceedings of the National Academy of Sciences of the United States of America* **109**, 15502–15507 (2012).

22. Oshio, K., Watanabe, H., Song, Y., Verkman, A. S. & Manley, G. T. Reduced cerebrospinal fluid production and intracranial pressure in mice lacking choroid plexus water channel Aquaporin-1. *FASEB journal: official publication of the Federation of American Societies for Experimental Biology* **19**, 76–78 (2005).

23. Nielsen, S. *et al.* Specialized membrane domains for water transport in glial cells: high-resolution immunogold cytochemistry of aquaporin-4 in rat brain. *J. Neurosci.* **17**, 171–180 (1997).

Acknowledgements

Author contributions

V.R.T., A.S.T., E.A.N. and M.N. planned the project, prepared figures 1–3 and wrote the main manuscript text. V.R.T. and A.S.T. performed in vivo and in situ experiments. B.P., M.T., J.J.I. and R.D. performed immunohistochemistry and contributed to the manuscript text and figures. All authors reviewed the manuscript.

Additional information